A combined anode nickel-titanium dioxide nanotube for photo-electrolysis

In this article we have studied a composite anode of nickel and an array of highly aligned TiO_2 nanotubes, obtained by a previous galvanostatic anodization treatment in an organic solvent. The electrochemical performances of the composite anode were estimated in a prototype of photo-electrolyser, that disclosed a good solar conversion efficiency together with a reduction of energy loss. The composite electrode makes our system able to work both in the dark and under solar light exposition, thus opening new outlooks for industrial-scale uses

DOI 10.12910/EAI2014-108

A. Pozio, A. Masci, M. Pasquali

Introduction

The photo-generation of hydrogen from the splitting of water using solar energy has been one of scientists' objectives since the early 1970s, when Fujishima et al. [1] gave an account of the generation of H_2 and O_2 in a photoelectrochemical cell (PEC) using a titanium oxide electrode brightened with UV light.

More recently, Gong et al. [2] gave birth to a new synthesis model for the TiO_2 nanotubes based on the anodic oxidation of a titanium foil in ammonium fluoride solutions. This method has paved the way to a new approach able to combine an easy preparation of the material with a full control of physical characteristics of the nano-system [3-6].

Due to the peculiar geometric shape of nanotubes, particularly applicable as photo-anode in a cell of photoelectrolysis [7], many studies have been addressed towards this application, arriving to report elevated values of UV photo-conversion efficiency for these nano-systems [8,9]. On the other hand, although many improvements have been reached, the high band-gap of titania limits the light adsorption only to a restricted UV region. [7]. Moreover, also the titania electro-catalytic activity for the oxygen evolution reaction (*OER*) is very small, if compared with that obtained on conventional metallic electrodes (Pt, Ni etc). This limits the use of the titanium oxide due to the low current density generated both in the conventional and photo-assisted modes. For this reason, a different approach can be beneficial, based on the use of a composite electrode able to guarantee a high electrocatalytic activity for the *OER*, but exploiting the photo-activity in order to decrease the power consumption. Such kind of electrode could be used in a photo-assisted electrolyser in the presence of a solar light source. Previously, most researchers have centered their study on the doping of TiO_2 nanostructures, mainly in order to shift the adsorption of light toward the visible energy region [10-23]. As an alternative, the usage of co-catalyst to increase in reactivity was first observed for the photo-conversion of water into H_2 and O_2 by means of the Pt-TiO_2 electrodes [24]. The presence of metals in a semiconductor can change the photo-catalytic process by changing the properties of the semiconductor surface. The metal can improve the yield of a specific product or the speed of the photo-catalytic reaction. At the same time, the metal can also be important be-

Contact person: Alfonso Pozio
alfonso.pozio@enea.it

cause of its electro-catalytic activity. Typical inorganic catalysts for water oxidation include oxides of nickel, ruthenium, cobalt and iridium, etc [25]. The deposition of NiO_x, IrO_x, CoO_x and RuO_x co-catalysts on n-semiconductors enhances the activity for oxygen evolution. In particular, Ni and Co oxides were found to be good catalysts in the alkaline environment [26,27]. In the past, Dinca et al. [27] introduced the self-assembly of a highly active nickel-based O_2 evolving catalyst that forms as a thin film on inert electrodes when aqueous solutions of Ni^{2+} salts are electrolyzed in the presence of phosphate or borate [44]. These authors pointed out that this catalyst can be produced *in situ* under mild conditions on a variety of conductive substrates, and it discloses high activity for *OER* at room temperature. This catalyst showed long-term stability in water without corrosion, thus permitting to store energy with devices that are inexpensive and with a high manufacturability. Besides, Shrestha et al. have loaded with Ni oxide nanoparticles self-organized TiO_2 nanotubes grown by anodization of titanium in glycerol-water electrolyte containing fluoride, by a simple technique of precipitation in chemical bath [28]. The synergy of the metal and semiconductor component is essential for enhancing the performance of nano-composites in the photo-catalysis process [29]. In this work we have tried a different *modus operandi*, the mechanical pairing of semiconductor/metal in order to produce a large surface electrode. We embedded the disks of TiO_2 nanotubes/titanium, directly into a porous nickel sheet, using a cold pressing method. The result was a PEC with a new innovative design, in which the anode is formed by a series of electrodes of TiO_2 nanotubes that are inserted tightly on porous nickel. Such coupling could allow to exploit both the electro-catalytic property of Nickel for the O_2 evolution and the photo-catalytic property of TiO_2. We have seen that the composite Nickel–TiO_2/Ti electrodes possess different properties with respect to the single component. The composite electrode could represent a valid alternative able to ensure the functioning of the anode in the photo-assisted (presence of UV) or conventional (without UV) mode. In our tests a prototype of electrolyser, with a large anode, has been examined in the direct sunlight to evaluate its performance.

Experimental

Materials and preparatives

Small disks (Ø 15 mm x 0.5 mm) of commercial titanium (Pure grade 3 - Titania, Italy) have been selected as substrate for the nanotube anodic growth. The unmodified sample (TiO_2/Ti) was prepared with the same methodology developed in other previous articles [9,30]. Briefly, after 3 min. pickling in a 1:3 HF/HNO_3 (Carlo Erba) diluted solution, the titanium disks have been placed into a three-electrode cell containing a 1 M KOH solution (Carlo Erba) and then subject to a 1 mA/cm^2 current density for 3 min. The counter-electrode was a platinum sheet, while the reference was a standard calomel electrode (SCE). The anodic growth of the nanotube arrays has been obtained in a two-electrode cell with a platinum counter electrode, using a glycol ethylene (Ashland) solution with 1 %wt. H_2O and 0.2 %wt. NH_4F, and applying 60 V for 3 h by means of a potenziostat/galvanostat PS251-2 (Aldrich). The current has been measured with a Keithley 2000 multimeter and acquired with a Madge-Tech Volt101 digital recorder, placed in series with a calibrated resistance (300 Ω) Leeds and Northrup (Figure 1).

After the anodization, the sample was washed in glycol ethylene and left overnight in a dry room. Then, in or-

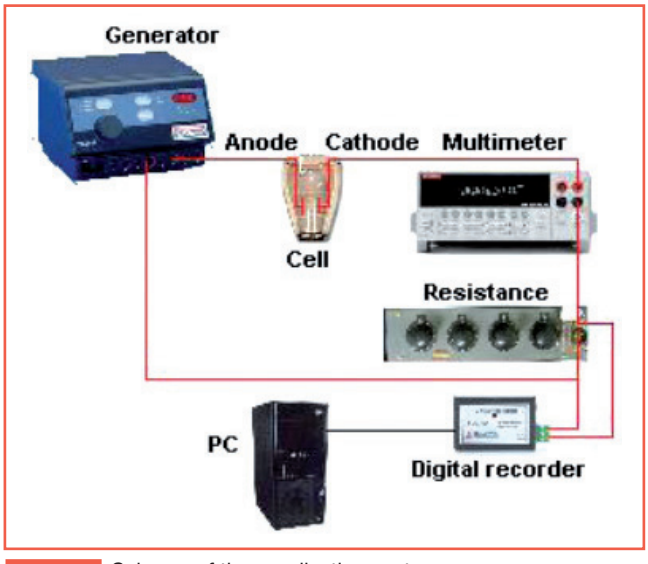

FIGURE 1 Scheme of the anodization system

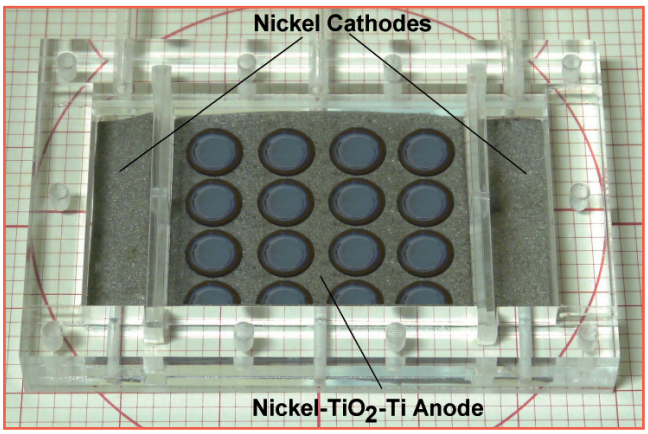

FIGURE 2 Photo-electrolysis cell with composite TiO_2/Ti-Nickel anode

der to transform amorphous TiO_2 nanotubes into the anatase phase, the samples were first heated at 90 °C in vacuum for 3 hours and subsequently placed into a tubular furnace (Lenton) for 1 h at 580 °C with a slope of 1 °C/min in air. Sixteen TiO_2/Ti samples were embedded in a porous nickel sheet. The titanium disks were placed on a 50 cm^2 foil of porous, ductile nickel (2 mm thickness) and cold embedded, by applying a pressure of 50 bar by means of a hydraulic press (ATS Faar). The final results was a 16-TiO_2/Ti disk well framed inside the porous structure, as shown in Figure 2.

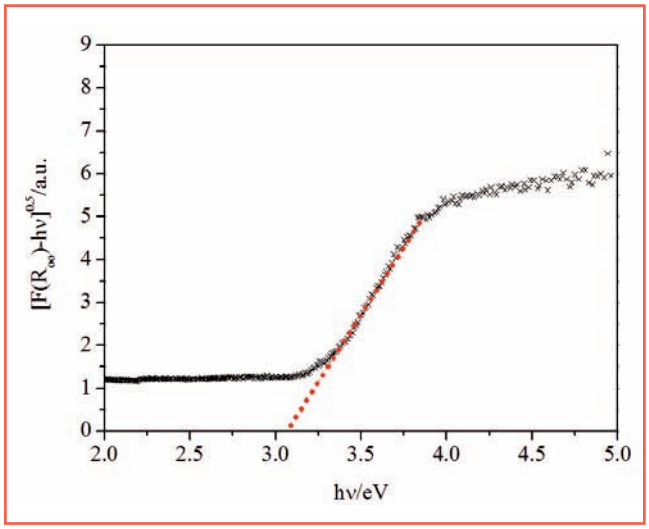

FIGURE 3 The transformed Kubelka-Munk function vs. energy of excitation source for TiO_2/Ti (×)

Electrochemical measurements

The electrochemical measurements on the composite 16-TiO_2/Ti-Nickel sample were executed using a home-made, plexiglas electrolysis cell (30 cm^3) (Figure 2). Photo-electrolysis Tests, UV or non-UV (dark), were performed on the cell, between 1.4 to 2.0 V, in a configuration with two electrodes (sample working/Ni counter) in potassium hydroxide, 1 M electrolyte, at room temperature.

The anodic and cathodic chambers were separated with a porous, gas-proof felt (Testori-Italy). During the photo-electrolysis, the cell was tested by direct exposition to sunlight all day long. The photo-current measurements were carried out by exposing the cell to direct sunlight, measuring the visible radiation and its UV-A component by means of a photo radiometer HD2302 (Delta-Ohm).

UV-vis absorption spectra

The diffuse reflectance spectrum of a single TiO_2/Ti sample disk was obtained using a Lambda 9 spectrophotometer, equipped with an integrating sphere. The reflectance data was converted to the absorption coefficient $F(R_{00})$ values according to the Kubelka-Munk equation [31,32]:

$$F(R_\infty) = \frac{(1-R_\infty)^2}{2R_\infty} \quad (1)$$

The absorption coefficient $F(R_{00})$ and the bandgap E_g are related through the equation [33]:

$$[F(R_\infty) * h\nu]^S = h\nu - E_g \quad (2)$$

where ν is the frequency, h is the Planck's constant, and S=0.5 for indirect bandgap material [7]. In this way, the plotting of $[F(R_\infty) * h\nu]^{0.5}$ vs. $h\nu$, the so-called Tauc plot, allows to obtain the optical band-gap by dropping a line from the maximum slope of the curve to the x-axis [34-37].

Results and discussion

Analysis of the absorbance spectra

The energy of band gap (Eg) of a single TiO_2/Ti sample disk was calculated using the Tauc plot (Figure 3), as previously described, obtaining a value of 3.096 eV corresponding to a wave length of 413 nm.

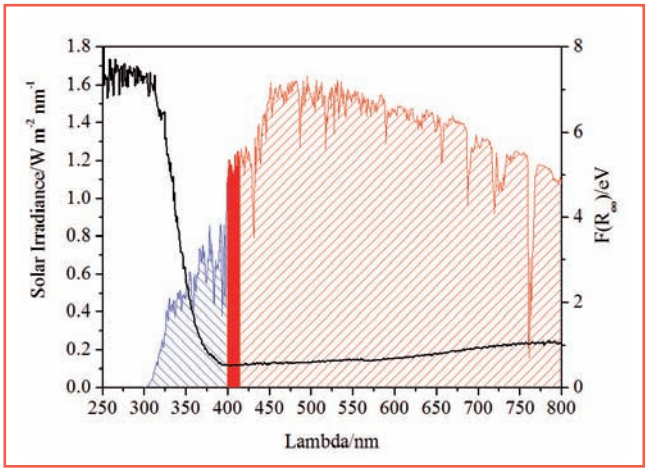

FIGURE 4 The global solar irradiance in the UV (▬) or Visible (▬) region [7] at AM 1.5 and absorption coefficient spectra of the TiO_2/Ti (▬) according to the Kubelka-Munk equation

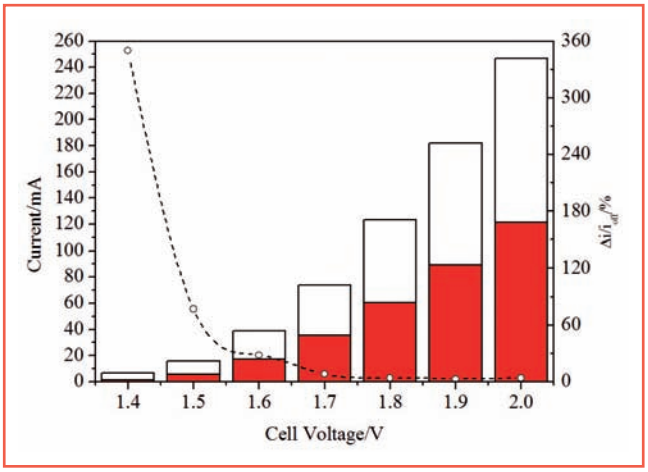

FIGURE 5 Current vs cell voltage with Ni-TiO_2/Ti anode at UV-on (□) and UV-off (■) and relative change of current density (– ○ –) in KOH 1 M at 25 °C, UV-A intensity 62 W m^{-2}

The global solar irradiance [7] at air mass 1.5 is showed in Figure 4 together with the diffuse absorbance spectra of a Ti/TiO_2 sample, obtained by the Kubelka-Munk equation. The titanium sample starts to absorb for λ≤413 nm but, with the main absorbance in the UV range 300÷400 (open blue area) that corresponds to about 5.95 % of solar global irradiance (among 300÷1050 nm). As can be seen from Figure 4, in the visible range 400÷413 nm, only a very small part (full red area) of the global solar irradiance (open red area) can be absorbed by the TiO_2 sample.

Analysis of the electrolysis cell performance

Figure 5 shows the electrolysis current obtained at different electrolysis cell voltages between 1.4-2.0 Volts, under on- and off-UV conditions, and the relative change of current with respect to the value i_{off}.

The measurement shows that using the anode composite Nickel-TiO_2/Ti within an electrolyser, additional photocurrent can be generated so as to produce hydrogen even at very low voltage values (i.e. 1.4 V). Particularly, the onset voltage of the electrolysis was decreased of about 100 mV, from 1.5 to 1.4 Volt in the presence of UV-A light. The efficiency of a hydrogen generator can be evaluated through the amount of energy consumed per cubic meter of hydrogen produced under standard temperature (25 °C) and pressure (1 atm) conditions. In such conditions, a conventional electrolyser with an efficiency of 100% (V_{Bias}=1.23 Volt) has an ideal energy consumption of about 2.7 kWh m^{-3}. With increasing applied voltage (V_{Bias}) the power consumption increases proportionately and the energy consumption, of course, depends inversely on temperature and directly on pressure (Figure 6).

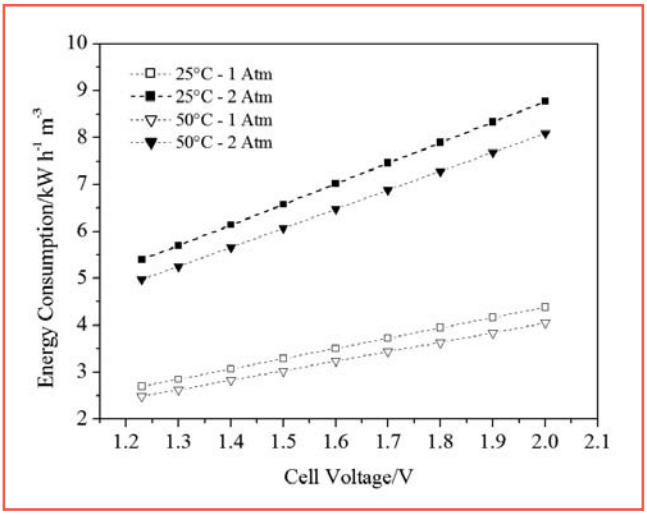

FIGURE 6 Energy consumption vs cell voltage at different pressure and temperature values

The energy consumption (kWh) for the electrolyser can be calculated as follows:

$$P = i_{off} V_{Bias} \times 10^{-3} \quad (3)$$

where i_{off} is the electrolysis current. For a photo-electrolyser, the energy consumption is always expressed by Eq. 3, which only considers the current supplied from the external generator (i_{off}), while the volume of hydrogen produced in cubic meters will be given by

$$V(H_2) = \frac{i_{on} 3600}{2F} RT \quad (4)$$

where the faradic yield is given by the total current (ion), F is the Faraday's constant, R the gas constant and T the temperature (°K). Therefore, the energy consumption of the photo-electrolyser, expressed in kWh m^{-3} will be given by the ratio of eqs. 3 and 4:

$$U(H_2) = \frac{P}{V(H_2)} = \cos t \frac{i_{off} V_{bias}}{i_{on}} \quad (5)$$

where all parameters are measured experimentally. As can be observed from Eq. 5, when the electrolyser is not illuminated the power consumption is simply given by the product of the voltage applied to a constant. If there is photo-current instead, consumption will decrease in proportion to the decrease of the ratio i_{off} /i_{on}. The value of the constant, of course, depends inversely on the temperature (2.02 to 50 °C, 2.19 to 25 °C and 2.39 at 0 °C) and directly on the pressure (4.38 to 2 bar abs and 25 °C). The energy consumption of the cell per m^3 of H_2 produced under standard conditions (Eq. 5) was calculated as a function of the voltage applied to the cell in the photo-assisted and conventional modes. Figure 7 shows that the maximum energy saving occurs at low voltage and tends to decrease asymptotically by increasing this up to 2 V, that is approx. 3.5%.

Based on the results so obtained, we performed measurements in conditions of direct exposure to the sunlight at two given voltages, 1.5 and 1.6 V, which are most visible photo-electrolytic effects.

Figure 8 shows the electrolysis current obtained at a cell voltage of 1.5 V and 1.6 V as a function of time under direct exposure to the sunlight, and the same current registered by shielding the cell. The figures also show the UV-A intensity over time. The trend evidences a maximum current in the central hours of the morning corresponding to the maximum UV-A. The UV-A radiation intensity was between 10.2÷24.5 W m^{-2}, representing approximately 3% of the incident global radiation. Finally, for both tests the energy consumption of the cell per m^3 of H_2 generated at 1 atm and 25 °C (Eq. 5) was achieved as a function of the voltage applied to the electrolyser in the photo-assisted or conventional mode (Figure 9). The graph also displays the reference value of energy consumption always evaluated in standard condi-

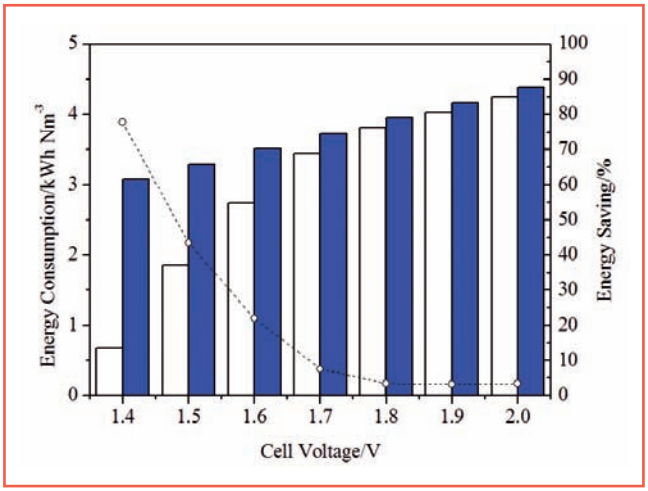

FIGURE 7 Energy consumption vs cell voltage with Nickel-TiO_2/Ti anode at UV-on (□) and UV-off (■) and relative energy saving (– ○ –) in KOH 1 M at 25 °C, UV intensity 62 W m^{-2}

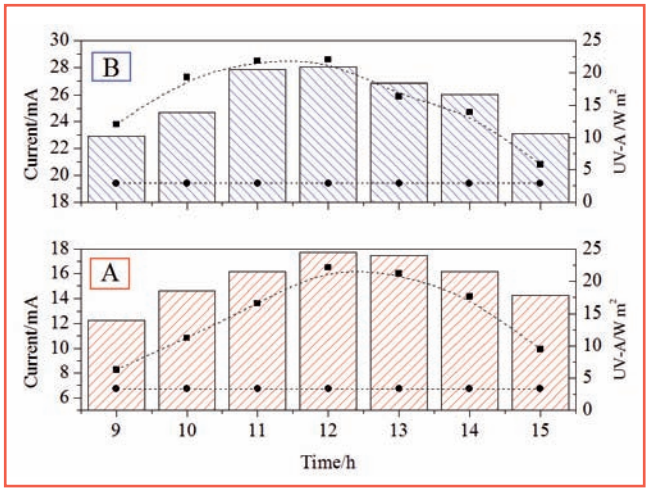

FIGURE 8 Electrolysis current vs time with direct solar exposition (– ■ –) or dark (– ● –) and UV-A intensity (bar) in KOH 1 M at 25 °C at 1.5 V (A) and 1.6 V (B)

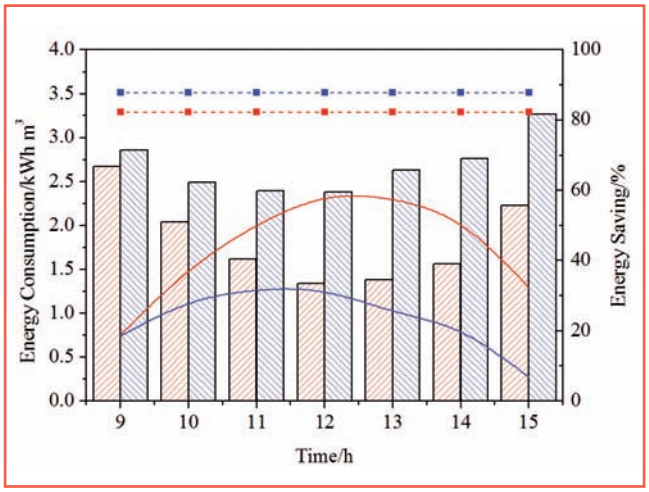

FIGURE 9 Photo-electrolyser energy consumption for m^3 of H_2 at 1.5 V (■) or 1.6 V (■) under direct solar exposition and relative energy saving (— or —). Dashed lines represent the energy consumption in dark at 1.5 V (3.29 kWh m^{-3}) (– ■ –) and at 1.6 V (3.51 kWh m^{-3}) (– ■ –)

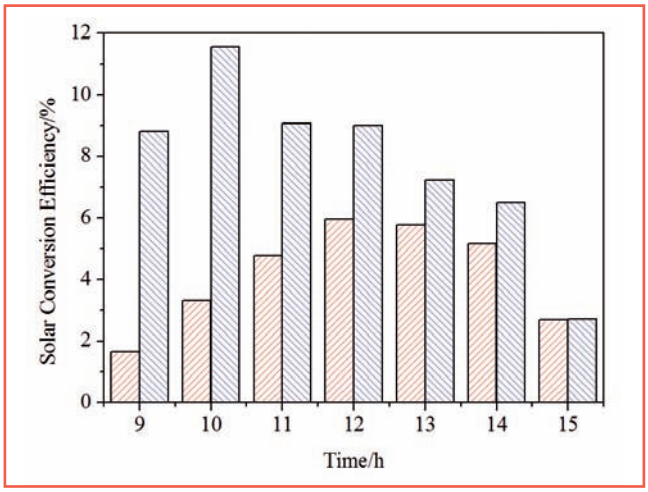

FIGURE 10 Solar conversion efficiency vs time with direct solar exposition at 1.5 V(■) and 1.6 V dark (■)in KOH 1 M at 25 °C

tions and in the absence of illumination at 1.5 V and 1.6 V. It is noted that the increase in light radiation produces an increase in the saving of energy, which is maximum in the central day hours and between 30÷60%, depending on the voltage applied to the PEC. Besides, the solar conversion efficiency η_c for the photo-electrolysers was calculated by the following expression [7]:

$$\eta_c = \frac{i_{ph}(1.23 - V_{bias})}{I_r A} \quad (6)$$

where V_{bias} is the voltage applied to the cell, i_{ph} the photo-current as the difference among i_{on} and i_{off}, A is the irradiated area (1.8×10^{-3} m^2) and I_r the UV-A irradiance intensity throughout the day (W m^{-2}).

Figure 10 shows the solar conversion efficiency at a V_{bias} of 1.5 and 1.6 volt throughout the day. In both cases, the efficiency shows a maximum value, respectively 12% at 1.6 V and 6% at 1.5 V. The mean efficiency throughout the day was 4.2% at 1.5 V and 7.8% at 1.6 V.

Conclusion

In this work, we have detailed a preliminary study for a new composite electrode made of porous nickel and an array of highly ordered TiO_2 nanotubes. The analysis reveals that the composite electrode could represent a valid alternative able to guarantee the functioning of the anode in both photo-assisted (presence of UV) and conventional (without UV) modes. In the case of the composite material, of course, the photo-electrochemical efficiency banks mainly on the component TiO_2/Ti, while the support of nickel ensures the catalytic activity in the absence of light. Moreover, a composite multi-anode was appraised with direct solar light exposition in a small photo-electrolyser. The system exhibited a good solar conversion efficiency together with a decrease in energy consumption. The results have demonstrated that a photo-electrolyser, operating with a cell voltage of 2 V and with a correct insulation guaranteed by its proper design and optimal management of the gas products, could reduce its energy demand by at least 3.5%.

Acknowledgments

We thank Dr. Alberto Mittiga (ENEA,Technical Unit for Renewable Energy Sources) for the Absorption Spectra measurements.

Alfonso Pozio, Amedeo Masci
ENEA, Technical Unit for Renewable Energy Sources

Mauro Pasquali
University of Rome "Sapienza"

References

1. A.K. Fujishima, K. Honda, Nature, 238 (1972) 37738
2. A. Gong, C.A. Grimes, O.K. Varghese, W. Hu, R.S. Singh, Z. Chen, E.C. Dickey, J. Mater. Res., 16 (2001) 3331-3334
3. G.K. Mor, O.K. Varghese, M. Paulose, N. Mukherjee, C.A. Grimes, J. Mater. Res., 18 (2003) 2588
4. Q. Cai, M. Paulose, O.K. Varghese, C.A. Grimes, J. Mater. Res., 20 (2005) 230
5. A.G. Kontos, A.I. Kontos, D.S. Tsoulkleris, V. Likodimos, J. Kunze, P. Schmuki, P. Falaras, Nanotechnology, 20 (2009) 045603
6. G.K. Mor, K. Shankar, M. Paulose, O.K. Varghese, C.A. Grimes, Nano Lett., 5 (2005) 191
7. C.A. Grimes, O.K. Varghese, S. Ranjan, The Solar Hydrogen Generation by Water Photoelectrolysis, (2008) Springer
8. K. Shankar, G.K. Mor, H.E. Prakasam, S. Yoriya, M. Paulose, O.K. Varghese, C.A. Grimes, Nanotechnology, 18 (2007) 065707
9. F. Mura, A. Masci, M. Pasquali, A. Pozio, Electrochimica Acta, 55 (2010) 2246–2251
10. Y. Wang, C. Feng, Z. Jin, J. Zhang, J. Yang, S. Zhang, J. Mol. Catal. A, 260 (2006) 1–3
11. A. Ghicov, J.M. Macak, H. Tsuchiya, J. Kunze, V. Haeublein, L. Frey, P. Schmuki, Nano Lett. 6 (2006) 1080-1082
12. A. Ghicov, J.M. Macak, H. Tsuchiya, J. Kunze, V. Haeublein, S. Kleber, P. Schmuki, Chem. Phys. Lett., 419 (2006) 426-429
13. K. Shankar, K.C. Tep, G.K. Mor, C.A. Grimes, J. Phys D, 39 (2006) 2361-2366
14. Q. Li, J.K. Shang, Env. Sci. Tech., 43 (2009) 8923-8929
15. L. Dong, Y. Ma, Y. Wang, Y. Tian, G. Ye, X. Jia, Mater. Lett., 63 (2009) 1598-1600
16. J. Xu, A. Yanhui, M. Chena, D. Fuc, Appl. Surf. Sci., 256 (2010) 4397-4401
17. J.H. Park, S. Kim, A.J. Bard, Nano Lett., 6 (2006) 24-28
18. K.S. Raja, M. Misra, V.K. Mahajan, T. Gandhi, P. Pillai, S.K. Mohapatra, J. Power Sources 161 (2006) 1450-1457
19. G. Wu, T. Nishikawa, B. Ohtani, A. Chen, Chem. Mater., 19 (2007) 4530-4537
20. S.K. Mohapatra, M. Misra, V.K. Mahajan, K.S. Raja, J. Phys. Chem. C, 111 (2007) 8677-8685
21. R. Hahn, A. Ghicov, J. Salonen, V.P. Lehto, P. Schmuki, Nanotechnology, 18 (2007) 105604
22. N. Lu, H. Zhao, J. Li, X. Quan, S. Chen, Separation and Purification Technology, 62 (2008) 668-673
23. Y. Su, S. Han, X. Zhang, X. Chen, L. Lei, Mat. Chem. Phys., 110 (2008) 239-246
24. A.L. Linsebigler, G. Lu, J.T. Yates, Chem. Rev., 95 (1995) 735-758
25. J. Yang, D. Wang, H. Han, C. Li, Accounts of Chemical Research, 46/8 (2013) 1900-1909
26. Y. Surendranath, M.W. Kanan, D.G. Nocera, J. Am. Chem. Soc., 132 (2010) 16501–16509
27. M. Dincă, Y. Surendranath, D.G. Nocera, PNAS, 107/23 (2010) 10337–10341
28. N.K. Shrestha, M. Yang, Y.C. Nah, I. Paramasivam, P. Schmuki, Electrochemistry Communications, 12 (2010) 254–257
29. P. Kamat, M. Flumiani, A. Dawson, Colloids and Surfaces A: Physicochemical and Engineering Aspects, 202 (2002) 269-279
30. F. Mura, A. Pozio, A. Masci, M. Pasquali, Electrochim., Acta 54 (2009) 3794–3798
31. G. Dupuis, M. Menu, Appl. Phys. A: Mater. Sci. Process., 83 (2006) 469
32. E.L. Simmons, Appl. Opt., 14 (1975) 1380-1386
33. B.E. Yoldas, D.P. Partlow, Thin Solids Films, 129 (1985) 1-14
34. G.K. Mor, O.K. Varghese, M. Paulose, C.A. Grimes, Adv. Funct. Mater., 15 (2005) 1291-1296
35. G. Burgeth, H. Kisch, Coord. Chem. Rev., 230 (2002) 41-47
36. Y. Yamada, N. Matsuki, T. Ohmori, H. Mametsuka, M. Kondo, A. Matsuda et al., Int. J. Hydrogen Energy, 28 (2003) 1167-9.
37. O. Khaselev, A. Bansal, J.A. Turner, Int. J. Of Hydrogen Energy, 26 (2001) 127-32